

Analysis and experimentation of a novel modulation technique for a dual-output WPT inverter

Manuele Bertoluzzo, Giuseppe Buja, *Life Fellow, IEEE*, and H. Dashora

Abstract—Dynamic wireless power transfer systems require to supply many transmitting coils arranged along a track, thus entailing the use of a large number of inverters or of complex devices that switch the power to the proper coils. This paper proposes a technique that allows to use a single inverter based on a three leg H-bridge to supply two coils with voltages having different and independently adjustable amplitudes. Moreover, the presented technique has the inherent ability of reducing the phase difference between the two output currents when the supplied loads are partially reactive, thus enhancing the power transfer capability of the inverter when both the transmitting coils are temporary coupled with the same pickup. After presenting the technique, the paper analyzes in details the functioning of the dual-output inverter in different load conditions, recognizes the boundaries of four different modes of operation, and gives some introductory hints about the control of the output voltages. The theoretical findings are validated by the results of experimental tests performed on a prototypal setup.

Index Terms— Inductive power transmission, Phase control, Voltage source inverters.

I. INTRODUCTION

WIRELESS power transfer (WPT) based on magnetic induction is the subject of advanced studies that aim at transferring power onboard electric vehicles running on suitable tracks [1]-[3]. Implementation of tracks requires to design carefully the transmitting coils [4], their reciprocal placement [5], and their supply system. The latter one could include a large number of inverters and hence it is mandatory to optimize its architecture. Some proposals have been presented to minimize the complexity and the cost of the supply infrastructure by using only one inverter and relying on the interaction between the transmitting coils to transfer energy to a load coupled to any of them [6], [7]. With this arrangement, however, it is not possible to control independently the coils as all of them are always energized. Other approaches are based on switches that forward the power supplied by the single inverter to the track coil or

coils that must be energized; the switches are implemented by static devices [8], [9] or by additional inductors whose cores are on purpose saturated to control the power transfer [10]; another solution exploits the inherent variation of the impedance of the coil coupled to the pickup to forward the supply power to it [11]. These approaches do not allow to control independently the power supplied to the energized coils and this could be a limiting factor if, depending on the distance between two subsequent transmitting coils and on their dimension, the pickup is temporary coupled simultaneously with two of them [5]. In this case, both the track coils contribute to the power transfer, which is maximum when the currents flowing in the coils are in phase so as to sum the magnetic fluxes linked with the pickup. The same requirement is found also in [12], where the currents in the two sub-coils of a DD coil are controlled separately. Besides the phase relation between the currents, it is also important to control independently their amplitude to maximize the WPT system (WPTS) efficiency; in [13], [14] the authors use separate inverters to supply the transmitting coils, increasing the complexity of the supply infrastructure, and requiring a data exchange between their control stages [13] to synchronize the phases of the output currents.

A solution to reduce the complexity of the infrastructure is presented in [15], where a PWM technique for a three legs inverter with two outputs is presented. The same scheme that uses three legs to supply two coils is generalized in [16] for the supply of multiple transmitting coils.

Considering that the surface vehicle standard J2954 issued by SAE [17] fixes to 85 kHz the nominal supply frequency f_s of the wireless charging station, the PWM technique proposed in [15] is not viable to control the amplitude of the high frequency inverter (HFI) output voltage. Instead, in WPT systems, the phase shift technique (PST) is commonly used [18], [19], even if some authors propose to supply the transmitting coils with a square-wave voltage [16].

An original technique for the command of the HFI power switched has been presented in [20]. This technique is derived from the PST but, differently from it, allows to supply simultaneously two coils with two voltages whose amplitudes

Manuscript received Month xx, 2xxx; revised Month xx, xxxx; accepted Month x, xxxx.

M. Bertoluzzo is with the Department of Industrial Engineering, University of Padova, Padova, 35131, Italy. (corresponding author +390498277923; e-mail: manuele.bertoluzzo@unipd.it).

G. Buja is with the Department of Industrial Engineering, University of Padova, Padova, 35131, Italy. (e-mail: giuseppe.buja@unipd.it).

H. Dashora is with the KPIT Technologies Ltd., Pune, Maharashtra, India. (e-mail: hemant.dashora@kpit.com).

are adjusted independently while maintaining their phase relation. Moreover, when the loads seen at the HFI outputs are partially reactive, this technique exhibits the inherent ability of adjusting the phases of the output voltages in order to reduce the phase difference between the two output currents. With respect to [20], this paper gives a much deeper mathematical analysis of the functioning and performance of the presented technique and, to this aim, uses the phasor notation, moreover, it reports the results of experimental tests.

The paper is organized as follows. Section II reviews the functioning and the limitations of the PST and introduces the phasor representation used in the subsequent Sections. Section III describes the proposed technique, and analyzes its operation with resistive loads. Section IV considers the effects of a partially reactive load on the amplitude and the phase of the output voltages. Section V demonstrates and quantifies the ability of the proposed technique to reduce the phase difference between the output currents. Section VI reports the results of tests performed on a prototypal WPTS. Section VII concludes the paper.

II. PHASE SHIFT TECHNIQUE

A single coil can be supplied using an HFI formed by the two legs LGa and LGc sketched in Fig. 1. According to PST, the power switches are commanded with square-wave gate signals to generate the two voltages v_{ao} and v_{co} plotted in the upper half of Fig. 2 with the red solid line and the green dash-dotted line, respectively. In drawing the figure and in the subsequent discussion, the effects of the dead-times and of the finite commutation times are neglected.

The actual waveform of the output voltage v_{ac} is imposed by the phase shift $\alpha_{a,ps}$ between the two voltages v_{ao} and v_{co} . The phase shift lies in the interval $(0, \pi)$. When $\alpha_{a,ps}=0$, v_{ao} and v_{co} are in phase and the output voltage v_{ac} is nullified; when $\alpha_{a,ps}=\pi$, v_{ao} and v_{co} are in phase opposition and v_{ac} has a square waveform with twice the amplitude of v_{ao} and v_{co} . In general, v_{ac} has the three-level waveform shown by the red solid line in the lower half of Fig. 2. In each semi period the length of the phase interval with non-zero voltage is equal to $\alpha_{a,ps}$.

Usually the coils of a WPTS are connected to suitable compensation networks made of reactive elements [21]. In Fig. 1 the compensation network is formed by the series capacitor C_a that resonates with the coil inductance L_a . The impedance $R_{ref,a}$ accounts for the coils parasitic resistance and the

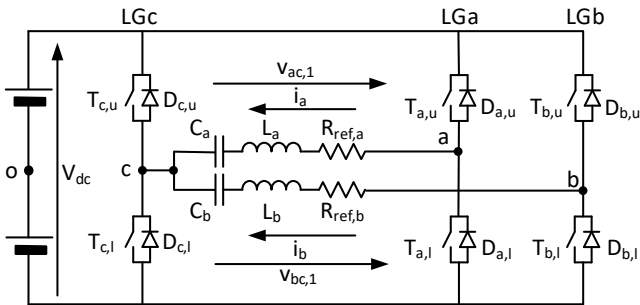


Fig. 1. Circuitual scheme of the single output HFI (legs LGa and LGc) and of the dual output HFI (all the three legs).

equivalent load of the receiving side of the WPTS reflected to the transmitting side. If the series resonance is enforced at the receiving side, $R_{ref,a}$ results purely resistive.

The series resonant compensation introduces a minimum of the reactance seen at the inverter output in correspondence with the supply frequency. Consequently, the inverter output current is nearly sinusoidal despite the quasi-square waveform of the output voltage. From this condition it derives that the analysis of the WPTS can be performed considering only the first harmonic of the output voltage rather than its actual waveform. The first harmonic $v_{ac,ps,fa}$ of $v_{ac,ps}$ is expressed by (1), where $\omega_s=2\pi \cdot f_s$ is the supply angular frequency.

$$v_{ac,ps,fa} = V_{ac,ps} \cos(\omega_s t + \theta_{vac,ps}). \quad (1)$$

The amplitude $V_{ac,ps}$ is

$$V_{ac,ps} = V_{dc} \frac{4}{\pi} \sin\left(\frac{\alpha_{a,ps}}{2}\right) \triangleq V_M \sin\left(\frac{\alpha_{a,ps}}{2}\right), \quad (2)$$

where V_M is the maximum first harmonic amplitude achievable at the inverter output with the given dc side voltage V_{dc} . The initial phase $\theta_{vac,ps}$ is measured with respect to the central point of the negative half period of v_{co} and results

$$\theta_{vac,ps} = \frac{\pi}{2} - \frac{\alpha_{a,ps}}{2}. \quad (3)$$

The first harmonic $v_{ac,ps,fa}$ is shown in the lower half of Fig. 2 using the thin red solid line.

To represent with more effectiveness the differences between the PST and the proposed technique, the phasor notation is introduced. Given the phase reference used in (1) and (3), the real axis of the phasor diagram corresponds to the opposite of the phasor of the first harmonic $v_{co,fa}$ of v_{co} .

The phasor of $v_{ac,ps,fa}$ is denoted as $\bar{V}_{ac,ps}$; its components are derived from (2) and (3) with some manipulations that involve the use of the double-angle and the half-angle formulas

$$\begin{cases} v_{ac,ps,Re} = \frac{V_M}{2} (1 - \cos(\alpha_{a,ps})) \\ v_{ac,ps,Im} = \frac{V_M}{2} \sin(\alpha_{a,ps}) \end{cases}. \quad (4)$$

By expressing $v_{ac,ps,Im}^2$ as a function of $v_{ac,ps,Re}^2$ and $v_{ac,ps,Re}$, the relation (5) is obtained

$$v_{ac,ps,Im}^2 + \left(v_{ac,ps,Re} - \frac{V_M}{2}\right)^2 = \left(\frac{V_M}{2}\right)^2, \quad (5)$$

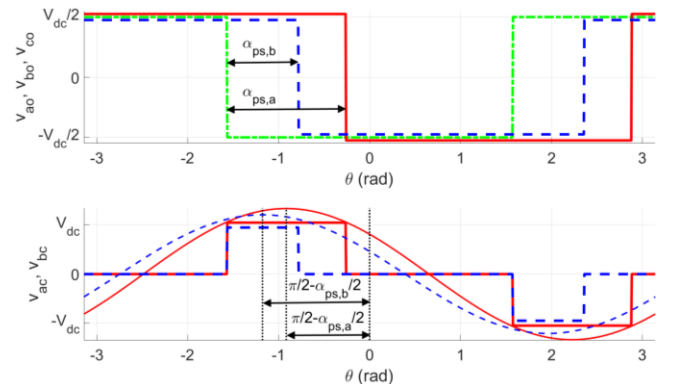


Fig. 2. Voltage waveforms generated by PST.

which reveals that while $\alpha_{a,ps}$ spans the interval $(0,\pi)$, the tip of $\vec{V}_{ac,ps}$ moves from $(0,0)$ to $(V_M,0)$ along the semi-circumference centered in $(V_M/2,0)$ and having radius equal to $V_M/2$, as shown in Fig. 3

The simultaneous supply of two or more coils can be performed using independent HFIs, however, it is possible to reduce the cost and the complexity of the WPTS by arranging the coils into pairs and supplying each pair using a three-legs HFI, as shown in Fig. 1. In this way, the power switches of the legs LGa and LGb are flown by the currents i_a and i_b , while LGc sustains the current i_c , equal to the sum of i_a and i_b .

Applying the PST to the gate command of LGb with respect to those of LGc, the amplitude $V_{bc,ps}$ can be adjusted independently from $V_{ac,ps}$, but, following from (3), if the phase shift angle $\theta_{ps,b}$ differs from $\theta_{ps,b}$, the phase $\theta_{vbc,ps}$ will be different from $\theta_{vac,ps}$, as shown in the lower half of Fig. 2 by the thin blue dashed line.

In the hypothesis that the reflected load is substantially resistive for both the coils, as it usually happens, a phase displacement between the supply voltages entails an about equal phase displacement between i_a and i_b , thus impairing the power transfer capability of the WPTS.

III. THE PARTIALLY IMPOSED VOLTAGE TECHNIQUE

The modulation technique presented in [20] is based on the hypothesis that the currents supplied by the dual-output HFI flow for the full supply period. As seen in the previous Section, this condition is verified provided that the WPTS operates in resonance. This technique allows to adjust independently the amplitudes V_{ac} and V_{bc} while maintaining the phase relation

$$\theta_{vac} - \theta_{vbc} = 0. \quad (6)$$

In the same way as PST, the switches of LGc are commanded with a 50% duty cycle, so that the voltage v_{co} , represented by the thick green dash-dotted line in the upper half of Fig. 4, is imposed during the full supply period. Differently from PST, there are not negligible intervals of the supply period during which neither the upper switch nor the lower one of LGa and/or LGb are closed. In these intervals, the actual voltages v_{ao} and v_{bo} are not imposed by the switching commands but are dictated by the currents at the inverter outputs, which force the conduction of either the upper or the lower free-wheeling diodes. For this reason, the presented technique is designed as

partially imposed voltage technique (PIVT).

More in details, as shown in the upper half of Fig. 4, PIVT closes the upper switch $T_{a,u}$ of LGa only for an interval centered around 0 and spanning α_a radians, and the lower switch $T_{a,l}$ of the same leg for an equal interval centered around π ; during these intervals the voltage v_{ao} is equal to V_{dc} and $-V_{dc}$, respectively, as highlighted by the thick red solid line. When both the switches are open, in agreement with the conventions of Fig. 1, a positive current i_a forces the conduction of the lower diode $D_{a,l}$ and drives v_{co} to $-V_{dc}$ while a negative i_a would flow through the upper diode $D_{a,u}$ driving v_{co} to V_{dc} . If i_a , which is considered sinusoidal, is in phase to $-v_{co,fa}$, as exemplified by the magenta dotted line, the waveform of v_{ao} results as reported in the upper half of Fig. 4, where the voltages due to the diode conduction are represented by the thin red dashed line. The output voltage $v_{ac}=v_{ao}-v_{co}$ is plotted in the lower half of Fig. 4, using the thick red solid line when the voltage is imposed by the switches and the thin red dashed line when it is driven by the diodes. Obviously, PIVT is used also to command the switches of LGb; if the current i_b is in phase to $-v_{co,fa}$, the voltages v_{bo} and v_{bc} have the waveforms plotted with the blue lines, the difference with respect to v_{ao} and v_{ac} being that the length of the switches conduction intervals is α_b instead of α_a .

The waveforms of v_{ac} and v_{bc} are the same obtained with the PST but their phase is different as they are symmetric with respect to $\theta=0$. Thanks to this symmetry it results

$$\theta_{vac} = \theta_{vbc} = 0 \quad (7)$$

for any pair of α_a and α_b so that (6) is always verified. By (7), the two voltages result in phase opposition to $v_{co,fa}$ and hence they are in phase to i_a and i_b .

Eq. (2) is used to find the amplitude of the first harmonic components of v_{ac} and v_{bc} . For v_{ac} , it is rewritten as

$$V_{ac,0} = V_M \sin\left(\frac{\alpha_a}{2}\right), \quad (8)$$

where the subscript “0” denotes that (8) refers to the condition of having i_a in phase to $v_{ac,fa}$.

While α_a varies in $(0,\pi)$, the tip of the phasor $\vec{V}_{ac,0}$ moves from $(0,0)$ to $(V_M,0)$ along the real axis of Fig. 3. The components of $\vec{V}_{ac,0}$ are

$$\begin{cases} v_{ac,0,Re} = V_M \sin\left(\frac{\alpha_a}{2}\right), \\ v_{ac,0,Im} = 0 \end{cases} \quad (9)$$

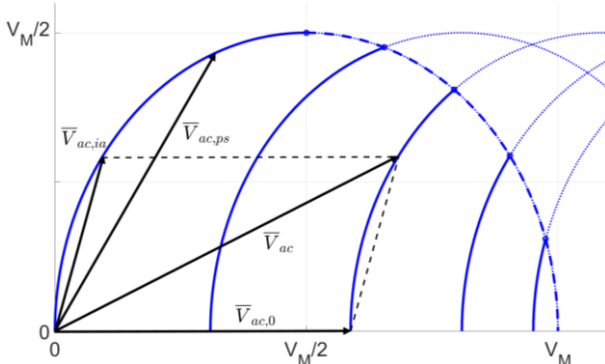


Fig. 3. Phasor representation of the output voltage.

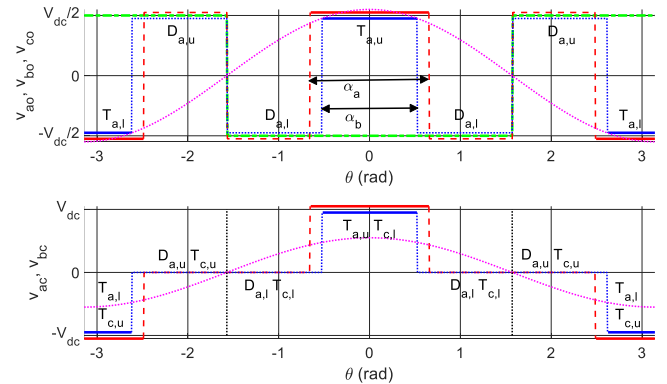


Fig. 4. Voltage waveforms generated by PIVT with $\theta_{ia}=\theta_{ib}=0$.

The results of this Section can be summarized by stating that if the loads seen at the HFI outputs are purely resistive, the currents i_a and i_b are in phase irrespectively from the output voltages.

IV. EFFECT OF LOAD REACTANCE

The hypothesis of having a purely resistive load at the inverter output cannot be assured in practical application because of the tolerance on the components of the compensation networks, their variations with ageing, the dependence of the self-inductances of the coils to their positions with respect to the pickup.

Any of these causes originates phase shifts between the currents i_a and i_b and the first harmonics $v_{ac,fa}$ and $v_{bc,fa}$ of the relevant voltages. In the subsequent analysis it is supposed that the phase shifts can take any value even if, in a practical application, only the interval $(-\pi/2, \pi/2)$ should be considered, otherwise the power would flow back from the load to the dc side of the HFI. In order to simplify the discussion, only the effect of a phase lag of i_a with respect to $-v_{co,fa}$ will be considered, with the awareness that the results can be easily adapted to the case of i_a leading $-v_{co,fa}$, and extended to the current i_b . Moreover, it is also supposed that $\alpha_a > 0$ whilst the generalization of the results to the case $\alpha_a = 0$ is reported in the next Section.

By analysis of Fig. 4, three modes of operation can be recognized: A) i_a changes its sign from negative to positive before $T_{a,u}$ is switched on; B) i_a changes sign while $T_{a,u}$ is on; C) i_a changes its sign after $T_{a,u}$ is switched off.

Each mode originates a different behavior and must be studied separately. In all the cases i_a is considered sinusoidal and is expressed as

$$i_a = I_a \cos(\omega_s t + \theta_{ia}). \quad (10)$$

A. $(\alpha_a/2 - \pi/2) < \theta_{ia} < 0$

This situation is exemplified in Fig. 5. By comparison with Fig. 4, it results that there are two more phase intervals where the HFI output voltage v_{ac} is different from zero. During the first interval, which begins at the falling edge of v_{co} and extends for a phase angle equal to $|\theta_{ia}|$, i_a forces the conduction of $D_{a,u}$ so that v_{ac} results equal to V_{dc} . During the second interval, which has the same phase length and begins at the rising edge of v_{co} , the conducting diode is $D_{a,l}$ and v_{ac} is equal to $-V_{dc}$.

The voltage v_{ac} can be expressed as the sum of the output voltage plotted in Fig. 4 and relevant to the case of $\theta_{ia} = 0$, and of the voltage $v_{ac,ia}$, plotted with the blue dotted line in the lower half of Fig. 5, which includes only the two additional conduction intervals originated by the reactive component of i_a . The waveform of $v_{ac,ia}$ is similar to that of Fig. 2 and hence the parameters of its first harmonic $v_{ac,ia,fa}$ are easily derived from (2) and (3) as

$$V_{ac,ia} = -V_M \sin\left(\frac{\theta_{ia}}{2}\right), \quad (11)$$

$$\theta_{vac,ia} = \frac{\pi}{2} + \frac{\theta_{ia}}{2}, \quad (12)$$

where θ_{ia} is negative because, by hypothesis, $(\alpha_a/2 - \pi/2) < \theta_{ia} < 0$.

Eqs. (11) and (12) shows that, differently from what happens with α_a , the angle θ_{ia} affects the phase of $v_{ac,ia,fa}$ besides its amplitude, and hence it effects the phase of $v_{ac,fa}$.

The phasor of $v_{ac,fa}$ can be decomposed as in Fig. 3 in two contributes

$$\bar{V}_{ac} = \bar{V}_{ac,0} + \bar{V}_{ac,ia} \quad (13)$$

The first of them is aligned with the real axis and has the components (9) while the components of $\bar{V}_{ac,ia}$, derived from (11) and (12) are

$$\begin{cases} v_{ac,ia,Re} = \frac{V_M}{2} (1 - \cos(\theta_{ia})) \\ v_{ac,ia,Im} = -\frac{V_M}{2} \sin(\theta_{ia}) \end{cases} \quad (14)$$

From the comparison of (14) with (4) and by remembering that θ_{ia} is negative it can be concluded that the tip of $\bar{V}_{ac,ia}$ moves on the same semi-circumference as the tip of $\bar{V}_{ac,ps}$. In the limit condition of $\alpha_a = 0$ and in the hypothesis that also in this case i_a flows for the full supply period, the constraint $(\alpha_a/2 - \pi/2) < \theta_{ia} < 0$ states that θ_{ia} could span the interval $(-\pi/2, 0)$ and that, consequently, the tip of \bar{V}_{ac} , which is equal to $\bar{V}_{ac,ia}$ if $\alpha_a = 0$, would move on the arc of the semi-circumference beginning at $(V_M/2, V_M/2)$ and ending at $(0, 0)$. This is denoted as the maximum arc.

In realistic operating conditions α_a is bigger than zero and as it increases, θ_{ia} can span a reducing angular interval so that the tip of $\bar{V}_{ac,ia}$ moves on shorter and shorter sections of the maximum arc, beginning at the point

$$\begin{cases} v_{ac,ia,Re,max} = \frac{V_M}{2} \left(1 - \sin\left(\frac{\alpha_a}{2}\right)\right) \\ v_{ac,ia,Im,max} = \frac{V_M}{2} \cos\left(\frac{\alpha_a}{2}\right) \end{cases} \quad (15)$$

and ending at $(0, 0)$. Eq. (15) is obtained from (14) by setting $\theta_{ia} = -\pi/2 + \alpha_a/2$.

From (13), (14), and (9), the components of the phasor \bar{V}_{ac} result

$$\begin{cases} v_{ac,Re} = \frac{V_M}{2} \left[2\sin\left(\frac{\alpha_a}{2}\right) + 1 - \cos(\theta_{ia})\right] \\ v_{ac,Im} = -\frac{V_M}{2} \sin(\theta_{ia}) \end{cases}; \quad (16)$$

from them, the amplitude and the phase of \bar{V}_{ac} are readily derived as

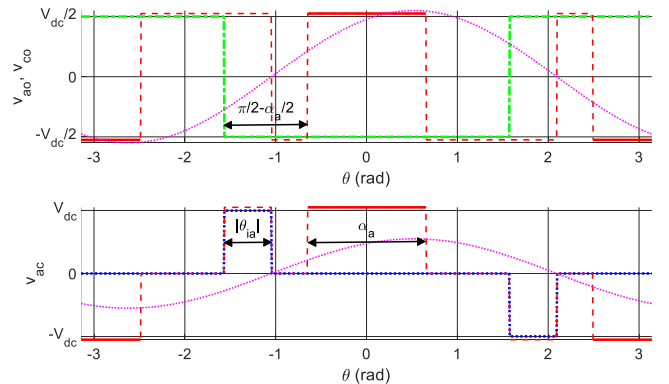


Fig. 5. Voltage waveforms generated by PIVT in mode A.

$$V_{ac} = \frac{V_M}{2} \sqrt{\left[2\sin\left(\frac{\alpha_a}{2}\right) + 1 - \cos(\theta_{ia})\right]^2 + [\sin(\theta_{ia})]^2} \quad (17)$$

$$\theta_{vac,1} = \text{atan} \left[-\frac{\sin(\theta_{ia})}{2\sin\left(\frac{\alpha_a}{2}\right) + 1 - \cos(\theta_{ia})} \right] \quad (18)$$

For a given value of α_a , V_{ac} results higher than $V_{ac,0}$ because of the contribute of $\bar{V}_{ac,ia}$, but in any case, V_{ac} never exceeds V_M , which is reached when $\alpha_a = \pi$ and $\bar{V}_{ac,ia}$ is null.

For any value of α_a in $(0, \pi)$, while θ_{ia} spans the interval $(\alpha_a/2 - \pi/2, 0)$, the tip of \bar{V}_{ac} moves on an arc originating at

$$\begin{cases} v_{ac,Re,max} = \frac{V_M}{2} \left(1 + \sin\left(\frac{\alpha_a}{2}\right)\right) \\ v_{ac,Im,max} = \frac{V_M}{2} \cos\left(\frac{\alpha_a}{2}\right) \end{cases} \quad (19)$$

and ending at $(V_M \sin(\alpha_a/2), 0)$. The origins of these arcs lie on the quarter of circumference drawn with the blue dash-dotted line in Fig. 3. It is denoted as limit arc because, together the maximum arc, it bounds the semi-circle where all the possible phasors \bar{V}_{ac} fall.

Fig. 3. reports an example of the decomposition of \bar{V}_{ac} according to (13) and all the possible positions of its tip for five different values of α_a . When $\alpha_a = 0$ the maximum arc on the left, expressed by (14), is obtained; as α_a increases the arcs origins move to the right on the limit arc and their length diminishes. Any two arcs intersect only outside the boundary semi-circumference and, consequently, for any given phasor \bar{V}_{ac} there is only one pair of α_a and θ_{ia} that realize it.

The analysis of the PIVT when i_a leads $-v_{co}$ and $0 \leq \theta_{ia} \leq (\pi/2 - \alpha_a/2)$ is readily derived from the previous results considering that in this situation the conduction intervals of the diodes are on the right of the power switches conduction intervals instead that on the left. As a consequence, the phase of $\bar{V}_{ac,ia}$ is negative and the phasor diagram of Fig. 3 must be redrawn symmetrically with respect to the real axis.

B. $(-\alpha_a/2 - \pi/2) \leq \theta_{ia} \leq (\alpha_a/2 - \pi/2)$

This mode is exemplified in Fig. 6. By comparison with Fig. 5, it results that now the intervals of diode conduction extend up to the turning on of the power switches. As a consequence, the output voltage v_{ac} results positive from $-\pi/2$ to α_a and negative from $\pi/2$ to $\pi + \alpha_a$ with a waveform that depends on α_a only, being the same that would have been obtained using the

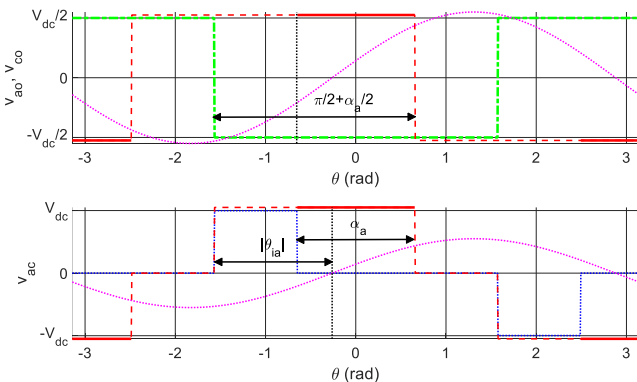


Fig. 6. Voltage waveforms generated by PIVT in mode B.

PST with $\alpha_{a,ps} = \pi/2 + \alpha_a/2$. The amplitude and the phase of $v_{ac,fs}$ are then expressed by (20) and (21), obtained from (2) and (3).

$$V_{ac} = V_M \sin\left(\frac{\pi}{4} + \frac{\alpha_a}{4}\right), \quad (20)$$

$$\theta_{vac} = \frac{\pi}{4} - \frac{\alpha_a}{4}. \quad (21)$$

The components of \bar{V}_{ac} are worked out manipulating (20) and (21) obtaining expressions equal to (19), thus demonstrating that while α_a spans the interval $(0, \pi)$, the tip of \bar{V}_{ac} lies on the limit arc.

As in the previous mode, if the current i_a leads $-v_{co,fa}$ and $(\pi/2 - \alpha_a/2) \leq \theta_{ia} \leq (\pi/2 + \alpha_a/2)$, the findings are still valid provided that the diagram of Fig. 3 is redrawn symmetrically with respect to the real axis.

C. $-\pi \leq \theta_{ia} \leq (-\alpha_a/2 - \pi/2)$

This mode happens when the diodes conduction enlarges the phase interval of non-zero v_{ac} beyond the end of the conduction interval of the power switches, as exemplified in Fig. 7.

The overall waveform of the output voltage v_{ac} is similar to that considered in situation A about $v_{ac,ia}$, consequently, V_{ac} and θ_{ac} are given by (11) and (12). However, in this case the interval spanned by θ_{ia} ranges from an angle smaller than $-\pi/2$ to $-\pi$ so that the tip of \bar{V}_{ac} lies on the limit arc instead that on the maximum arc.

If $0 \leq \theta_{ia} \leq (\pi/2 - \alpha_a/2)$, the symmetry of phasor diagram with respect to the real axis holds also in this mode.

V. PHASE ADJUSTING PROPERTY OF PIVT

The phase adjusting property of the PIVT can be easily figured by conceiving an ideal experiment. Let's suppose that the equivalent loads at the HFI outputs are both resistive so that the phase displacements $\Delta\theta_{La}$ and $\Delta\theta_{Lb}$ between the output currents i_a and i_b and the relevant voltages $v_{ac,fa}$ and $v_{bc,fa}$ are zero. Then, there are no additional conduction intervals of the free-wheeling diodes and the phases θ_{vac} and θ_{vbc} of the output voltages are zero; being $\Delta\theta_{La} = \Delta\theta_{Lb} = 0$, the same holds also for θ_{ia} , and θ_{ib} .

If, for any reason, the equivalent load connected at the a-c output of the HFI becomes partially inductive, i_a starts lagging $v_{ac,fa}$ and $\Delta\theta_{La}$ becomes negative. The lag of i_a originates additional conduction intervals for the diodes which, in turn, forces $v_{ac,fa}$ to lead $v_{bc,fa}$ of the phase angle $\theta_{vac} > 0$. Being

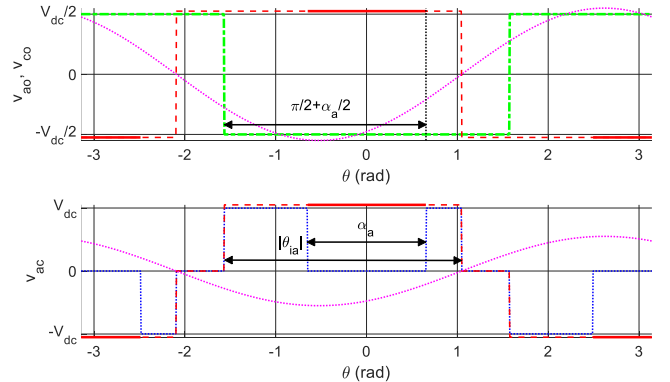


Fig. 7. Voltage waveforms generated by PIVT in mode C.

understood that $\Delta\theta_{La}$ is dictated by the equivalent load and independent from θ_{vac} , the phase advance of $v_{ac,fa}$ shifts i_a forward of the same phase angle. Then the resulting phase lag of i_a , equal to

$$\theta_{ia} = \Delta\theta_{La} + \theta_{vac}, \quad (22)$$

is smaller than it would have been if θ_{vac} had remained equal to 0, thus reducing the phase displacement between i_a and i_b . This result holds even if $\Delta\theta_{La} > 0$ or if the reactive load is connected to the b-c output of the HFI.

Eqs. (17)-(18), which hold in mode A, and (11)-(12), relevant to mode C, use θ_{ia} as independent variable to work out θ_{vac} , thus making difficult to apply directly (22) to obtain θ_{ia} . To circumvent this difficulty, it is useful to remind that usually the control algorithm of a WPT generates the reference for the amplitude of i_a and manipulates V_{ac} adjusting α_a to track it. Thus, in the subsequent considerations V_{ac} is considered as a given parameter V_{ac}^* and θ_{ia} is computed as a function of both V_{ac}^* and $\Delta\theta_{La}$. As a byproduct of the procedure, α_a is obtained as well, showing that in some conditions there is not any α_a able to implement the required V_{ac}^* , thus finding the boundaries of the operating region where PIVT can be actually controlled.

The computation of θ_{ia} begins by hypothesizing that the PIVT is operating in mode A. Using (22) to express θ_{vac} , the components of \vec{V}_{ac} are by definition equal to

$$\begin{cases} v_{ac,Re} = V_{ac}^* \cos(\theta_{ia} - \Delta\theta_{La}) \\ v_{ac,Im} = V_{ac}^* \sin(\theta_{ia} - \Delta\theta_{La}) \end{cases} \quad (23)$$

The second of (23) can be expanded in

$$v_{ac,Im} = V_{ac}^* [\sin(\theta_{ia}) \cos(\Delta\theta_{La}) - \cos(\theta_{ia}) \sin(\Delta\theta_{La})]. \quad (24)$$

Equating (24) to the second of (16) it is possible to derive a relation between θ_{ia} and $\Delta\theta_{La}$ as

$$\theta_{ia} = \text{atan} \left[\frac{\sin(\theta_{ia})}{\cos(\theta_{ia})} \right] = \text{atan} \left[\frac{\sin(\Delta\theta_{La})}{\cos(\Delta\theta_{La}) + \frac{1}{2} \frac{V_M}{V_{ac}^*}} \right]. \quad (25)$$

Eq. (25) states that $|\tan(\theta_{ia})| < |\tan(\Delta\theta_{La})|$ and that, consequently, $|\theta_{ia}| < |\Delta\theta_{La}|$, as expected. Moreover, (25) shows that for V_{ac}^* very small the phase adjusting is most effective because $\text{atan}(\theta_{ia})$ is small. If, instead, V_{ac}^* increases the phase adjusting is less effective.

Once θ_{ia} is obtained by (25), it is inserted in the first of (23) to compute $v_{ac,Re}$; then, θ_{ia} and $v_{ac,Re}$ are used in the first of (16) to work out α_a in the form

$$\alpha_a = 2a \sin \left(\frac{v_{ac,Re}}{V_M} + \frac{\cos(\theta_{ia})}{2} - \frac{1}{2} \right). \quad (26)$$

If $\alpha_a > 0$ and $(\alpha_a/2 - \pi/2) < \theta_{ia} < 0$ the hypothesis of operating in condition A is verified and the values obtained from (25) and (26) are correct. Otherwise mode B is considered.

In mode B, the phasor \vec{V}_{ac} is completely defined by α_a and so, being its amplitude V_{ac}^* given, by (20) it results

$$\alpha_a = 4 \left[a \sin \left(\frac{V_{ac}^*}{V_M} \right) - \frac{\pi}{4} \right]. \quad (27)$$

Once obtained α_a , it is substituted in (21) to find θ_{vac} and then, by (22) θ_{ia} is readily worked out. In this mode, α_a must be

positive and θ_{ia} must satisfy the condition $(-\alpha_a/2 - \pi/2) \leq \theta_{ia} \leq (\alpha_a/2 - \pi/2)$, otherwise mode C is checked

In mode C, the actual output voltage cannot be controlled because it depends on the conduction of the diodes rather than on the power switches commands. From (12) and (22), θ_{ia} is computed as a function of the phase displacement due to the load obtaining

$$\theta_{ia} = 2\Delta\theta_{La} + \pi; \quad (28)$$

then, using (11) and (12), \vec{V}_{ac} is derived.

The phase displacement α_a can assume any value between 0 and $-2(\theta_{ia} - \pi/2)$ without affecting the PIVT functioning. If α_a exceeds the maximum value, then mode B occurs. Instead, if α_a is equal to 0 a particular case of mode A happens. This mode is denoted as D and its analysis is readily performed recognizing that (16) changes into (14), which in turn comes from (11) and (12). Then the PIVT functioning is described by (11), (12) and (28), like in mode C but with the additional condition of having $\alpha_a = 0$.

Fig. 8 reports the plots of θ_{ia} as a function of $\Delta\theta_{La}$ for different values of the V_{ac}^*/V_M ratio. When $\Delta\theta_{La}$ is equal to zero, obviously θ_{ia} is equal to 0 as well, independently from the value of V_{ac}^* , and so all the curves begin at the origin of the graph. Initially PIVT operates in mode A and, according to (25), the phase compensation effect is stronger with small values of V_{ac}^* . This is reflected in Fig. 8, where the four different blue solid lines, each of them relevant to mode A with a different value of V_{ac}^* , show that for a given $|\Delta\theta_{La}|$ the corresponding $|\theta_{ia}|$ is always smaller, and that their difference increases as V_{ac}^* decreases. As θ_{ia} becomes more negative, the contribution of the additional conduction intervals to the overall amplitude V_{ac} increases and α_a must be reduced to maintain it equal to V_{ac}^* . At this point, two different evolutions are possible:

- 1) It happens that α_a must be set to zero while $|\theta_{ia}| < \pi/2$ thus passing to mode D. It is represented by the magenta dotted segment where three of the blue solid line merge. If $\Delta\theta_{La}$ decreases further, the diodes conduction intervals enlarge even more and when their angular span exceeds $\pi/2$, mode C is enforced and the $(\Delta\theta_{La}, \theta_{ia})$ pair moves on the green dash-dotted segment.
- 2) If V_{ac}^* is high enough, the enlarging diodes conduction intervals merge with the shrinking power switches

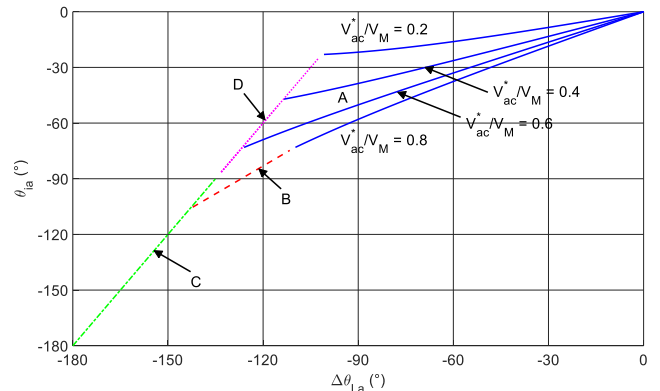


Fig. 8. Phase correction property of PIVT.

Table I. WPTS parameters

Parameter	Symbol	Value
Track coil, pickup, and inductor self-inductance	L_a, L_b, L_{pu}	120 μ H
Resonant capacitor	$C_{a,N}, C_{b,N}, C_{pu,N}$	29 nF
Mutual inductance	M	30 μ H
Supply angular frequency	ω	$2\pi \cdot 85000$ rad/s
DC bus voltage	V_{DC}	200 V

conduction intervals before the latter ones reduce to zero thus originating situation B, represented by the red dashed line. A further decrease of $\Delta\theta_{La}$ forces α_a to be set to zero, but now condition $|\theta_{ia}| > \pi/2$ holds and the PIVT moves from mode B to mode C without passing through mode D.

VI. EXPERIMENTAL RESULTS

The PIVT has been tested in an experimental setup [22] that includes an HFI whose output voltage v_{ac} supplies a series-compensated transmitting coil coupled with its pickup. The pickup is series-compensated as well, and is connected to a rectifier that, in turn, supplies a resistive load that emulates the EV battery. The HFI output voltage v_{bc} supplies a coil with a series compensation capacitor and a resistive load. This arrangement emulates the behavior of another track coil and at the same time maintains a constant resistive equivalent load at the HFI output in order to have i_b in phase to $v_{bc,fa}$ and perform the test in the same condition considered in the previous Sections. The transmitting coil, the pickup and the inductor have the same inductance; it is reported in Tab. I together with other parameters of the setup.

The HFI is controlled by a Texas microcontroller TMS320F28335 [23] and PIVT has been implemented using three of its six modules devoted to the generation of PWM signals.

The tests have been performed by increasing step by step the capacitance of the resonant capacitor connected to the track coil up to reaching twice its nominal value. The amplitude of both i_a and i_b has been maintained around 5A adjusting V_{ac} and V_{bc} though α_a and α_b . For each test, the samples of the waveforms of v_{ac} , v_{bc} , i_a and i_b have been acquired by means of a digital oscilloscope Tektronix TDS 5034. As an example, the waveforms relevant to the test performed with $C_a = 1.625 C_{a,N}$ are plotted in Fig. 9. The figure clearly shows the additional conduction intervals due to the phase lag $\Delta\theta_{La}$ of i_a with respect to v_{ac} , which have been predicted and described in the

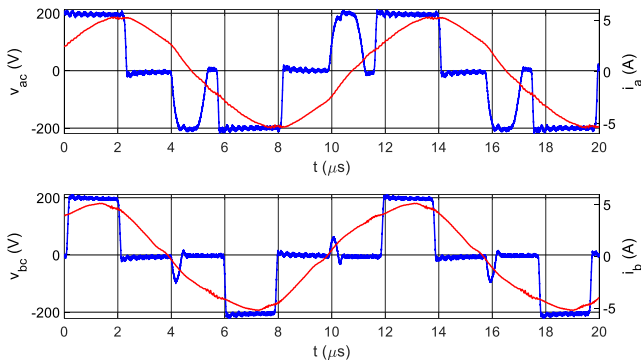

 Fig. 9. HFI output voltages and currents with $C_a = 1.625 C_{a,N}$.

Table II. Experimental results

$C_a/C_{a,N}$	V_{ac}/V_M	θ_{ia} ($^\circ$)	$\Delta\theta_{La}$ ($^\circ$)	θ_{ib} ($^\circ$)
1.000	0.4866	-0.3035	-2.1467	1.3282
1.125	0.5258	-8.9249	-20.7071	1.0642
1.250	0.5723	-15.9997	-32.4582	0.7766
1.375	0.6092	-21.4620	-40.0055	0.8392
1.500	0.6828	-26.0227	-45.2486	0.5198
1.625	0.7427	-30.0962	-49.2350	0.0802
1.750	0.8009	-32.7550	-52.0537	0.0568
1.875	0.8726	-34.8830	-54.2154	0.1543
2.000	0.9244	-37.4369	-56.2115	0.0872

section IV.A and Fig. 5. The spikes in the waveform of v_{bc} are due to the dead time of 0.5μ s inserted between the turning off and on of the power switches of LGb. The same dead time exists also for LGa, but its effect is not visible in the waveform of v_{ac} because it merges with the additional conduction intervals.

The waveform samples have been processed by a Matlab script to work out the amplitude and the phase of their first harmonic components obtaining the results listed in Tab. II. Following from the consideration of Section II and III, if the load seen at the HFI b-c output is purely resistive, $v_{bc,fa}$ results in phase to $-v_{co,fa}$ and hence it has been used as phase reference for the other quantities instead of $-v_{co,fa}$ without impairing the results of the previous Sections.

According to the last column of Tab. II, i_b results nearly perfectly in phase to $v_{bc,fa}$ thus confirming the initial hypothesis of having a resistive equivalent load at the b-c output of the HFI. The second column shows how V_{ac} has been increased to maintain a constant amplitude of i_a across the increasing impedance of the equivalent load. The fourth column reveals that $|\Delta\theta_{La}|$ never exceeds $\pi/3$ and that consequently, according to Fig. 8, the PIVT always operate in mode A.

Eq. (25) has been used to obtain the nine blue lines plotted in Fig. 10. Each of them corresponds to one value of V_{ac}/V_M given in Tab. II and to $\Delta\theta_{La}$ spanning the interval $(-\pi/3, 0)$. Indeed, Fig. 10 can be considered as a magnification of the upper-right part of Fig. 8. The blue circles are obtained inserting in (25) the $(V_{ac}/V_M, \Delta\theta_{La})$ pairs from Tab. II; each of them lies on a different line and represents the theoretical value of θ_{ia} . The red cross, instead, correspond to the experimental value of θ_{ia} , given by the third column of Tab. II.

Analysis of Fig. 10 shows that results from the experiments match very well with the expected ones and that PIVT is

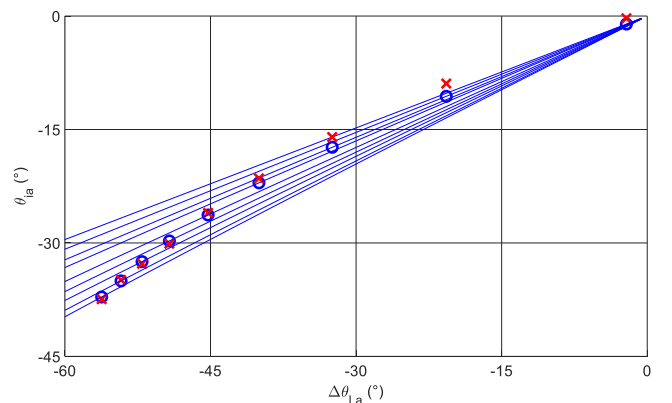


Fig. 10. Theoretical and experimental results comparison.

actually able to reduce the phase displacement between the currents when a reactive equivalent load is connected to the HFI outputs.

VII. CONCLUSIONS

The paper proposed a command technique for a three-leg HFI that allows the simultaneous supply of two track coils of a WPTS. The amplitudes of the voltages supplying the two coils can be adjusted independently while maintaining the coil currents in phase for resistive HFI loads and reducing the current phase difference under the onset of a reactive component of the loads. The proposed technique has been deeply analyzed mathematically and then substantiated by experimental tests performed on a prototypal WPTS.

REFERENCES

- [1] S.Li and C.C.Mi, "Wireless power transfer for electric vehicle applications," *IEEE Journal of Emerging and Selected Topics in Power Electronics*, vol. 3, no. 1, pp. 4-17, March 2015.
- [2] V. Cirimele, M. Diana, F. Freschi, and M. Mitolo, "Inductive power transfer for automotive applications: state-of-the-art and future trends," *IEEE Transactions on Industry Applications*, vol. 54, no. 5, pp. 4069-4079, Sept.-Oct. 2018, doi: 10.1109/TIA.2018.2836098.
- [3] R. Tavakoli and Z. Pantic, "Analysis, design, and demonstration of a 25-kW dynamic wireless charging system for roadway electric vehicles," *IEEE Journal of Emerging and Selected Topics in Power Electronics*, vol. 6, no. 3, pp. 1378-1393, Sept. 2018.
- [4] H.K. Dashora, G. Buja, M. Bertoluzzo, R. Pinto, and V. Lopresto, "Analysis and design of DD coupler for dynamic wireless charging of electric vehicles," *Journal of Electromagnetic Waves and Applications*, vol. 32, no. 2, pp. 170-189, 2018.
- [5] G. Buja, M. Bertoluzzo and H.K. Dashora, "Lumped track layout design for dynamic wireless charging of electric vehicles," *IEEE Transactions on Industrial Electronics*, vol. 63, no. 10, pp. 6631-6640, Oct. 2016.
- [6] C. Cheng, Z. Zhou, W. Li, C. Zhu, Z. Deng, and C. C. Mi, "A multi-load wireless power transfer system with series-parallel-series compensation," *IEEE Transactions on Power Electronics*, vol. 34, no. 8, pp. 7126-7130, Aug. 2019, doi: 10.1109/TPEL.2019.2895598.
- [7] Y. Wang, S. Zhao, H. Zhang and F. Lu, "High-efficiency bilateral S-SP compensated multiloop IPT system with constant-voltage outputs," *IEEE Transactions on Industrial Informatics*, vol. 18, no. 2, pp. 901-910, Feb. 2022, doi: 10.1109/TII.2021.3072394.
- [8] L. Shuguang, Y. Zhenxing and L. Wenbin, "Electric vehicle dynamic wireless charging technology based on multi-parallel primary coils," in Proc. of 2018 IEEE Int. Conf. on Electronics and Communication Engineering (ICECE), 2018, pp. 120-124.
- [9] 9C. Wang, C. Zhu, K. Song, G. Wei, S. Dong and R. G. Lu, "Primary-side control method in two-transmitter inductive wireless power transfer systems for dynamic wireless charging applications," in Proc. of IEEE PELS Workshop on Emerging Technologies: Wireless Power Transfer (WoW), 2017, pp. 1-6.
- [10] J. Zhao, Y. Zhang and L. Qi, "Design and analysis of a flexible multi-output wireless power transfer system with variable inductor," in Proc. of 2021 IEEE Energy Conversion Congress and Exposition (ECCE), 2021, pp. 1559-1564, doi: 10.1109/ECCE47101.2021.9595052.
- [11] H.K. Dashora, M. Bertoluzzo and G. Buja, "Reflexive properties for different pick-up circuit topologies in a distributed IPT track," in Proc. of IEEE Int. Conf. on Industrial Informatics (INDIN), 2015, pp. 69-75.
- [12] M. Bertoluzzo, G. Buja, and H. Dashora, "Avoiding null power point in DD coils", in Proc. of IEEE PELS Workshop on Emerging Technologies: Wireless Power (WoW), 2019, pp. 1-6.
- [13] S. Huh and D. Ahn, "Two-transmitter wireless power transfer with optimal activation and current selection of transmitters," *IEEE Transactions on Power Electronics*, vol. 33, no. 6, pp. 4957-4967, June 2018, doi: 10.1109/TPEL.2017.2725281.
- [14] D. -H. Kim and D. Ahn, "Maximum efficiency point tracking for multiple-transmitter wireless power transfer," *IEEE Transactions on Power Electronics*, vol. 35, no. 11, pp. 11391-11400, Nov. 2020, doi: 10.1109/TPEL.2019.2919293.
- [15] D. Jang, "PWM methods for two-phase inverters," *IEEE Industry Applications Magazine*, vol. 13, no. 2, pp. 50-61, March-April 2007.
- [16] Y. Zhang et al., "Free positioning wireless charging system based on tilted long-track transmitting coil array," *IEEE Transactions on Circuits and Systems II: Express Briefs*, doi: 10.1109/TCSII.2022.3177617.
- [17] SAE International, "Wireless power transfer for light-duty plug-in/electric vehicles and alignment methodology", Oct. 2020, [Online] Available: https://saemobilus.sae.org/content/J2954_202010/, last accessed: 06/06/2022.
- [18] C. Carretero, O. Lucia, J. Acero and J. M. Burdío, "Phase-shift control of dual half-bridge inverter feeding coupled loads for induction heating purposes," *Electronics Letters*, vol. 47, no. 11, pp. 670-671, May 2011.
- [19] M.H. Rashid, "Power Electronics circuits, devices, and applications," Third edition, Pearson/Prentice-Hall Publications, 2004.
- [20] H. Dashora, M. Bertoluzzo, and G. Buja, "Dual-output inverter with phase correction ability for dynamic WPT track supply," in Proc. of IECON 2019 - 45th Annual Conference of the IEEE Industrial Electronics Society, 2019, pp. 6349-6354, doi: 10.1109/IECON.2019.8927534.
- [21] W. Zhang and C.C. Mi, "Compensation Topologies of high-power wireless power transfer systems," *IEEE Transactions on Vehicular Technology*, vol. 65, no. 6, pp. 4768-4778, June 2016.
- [22] G. Buja, M. Bertoluzzo and K. N. Mude, "Design and experimentation of WPT charger for electric city car," *IEEE Transactions on Industrial Electronics*, vol. 62, no. 12, pp. 7436-7447, Dec. 2015, doi: 10.1109/TIE.2015.2455524.
- [23] Texas Instruments, "TMS320x2833x, TMS320x2823x Technical Reference Manual", March 2020, [Online] Available: <https://www.ti.com/lit/ug/sprui07/sprui07.pdf?ts=1657112036889>, last accessed: 06/07/2022.



Manuele Bertoluzzo received the M.S. degree in electronic engineering and the Ph.D. degree in industrial electronics and computer science from the University of Padova, Padova, Italy, in 1993 and 1997, respectively. Since 2015, he has been an Associate Professor at the Department of Electrical Engineering, University of Padova and holds the lectureship of road electric vehicles and systems for automation. He is involved in analysis and design of power electronics systems, especially for wireless charging of

electric vehicles battery.



Giuseppe Buja (M'75-SM'84-F'95-LF'13) received the "Laurea" degree with honors in power electronics engineering from the University of Padova, Padova, Italy, where he is currently a senior research scientist. He has carried out an extensive research work in the field of power and industrial electronics, originating the modulating-wave distortion and the optimum modulation for pulse-width modulation inverters. His current research interests are automotive electrification, including wireless charging of electric vehicles, and grid-integration of renewable energies.



Hemant Kumar Dashora (M'16) received the B.E. degree in electrical engineering from the University of Rajasthan, Jaipur, India, in 2009, and the M.Tech. degree in electrical engineering from IIT Kharagpur, Kharagpur, India, in 2011. He was a Senior Engineer with the General Motors Technical Centre, Bangalore, India, for almost 3 years. He focused on modeling and simulation of a complete architecture of hybrid and electric vehicles to analyze their fuel economy, performance, and durability. His current research interests include dynamic wireless charging of electric vehicles, coupling coil and power supply analysis.